Cracks induced by magnetic ordering in the antiperovskite $ZnNMn_3$

W. S. Kim,[1] E. O. Chi,[1] J. C. Kim,[1] N. H. Hur,[1,*] K. W. Lee,[2] and Y. N. Choi[3]
[1]*Center for CMR Materials, KRISS, Yusong, P.O. Box 102, Daejon 305-600, Korea*
[2]*Superconductivity Laboratory, KRISS, Yusong, P.O. Box 102, Daejon 305-600, Korea*
[3]*Neutron Physics Department, HANARO Center, KAERI, Yusong, Daejon 305-600, Korea*
(Received 1 August 2003; published 7 November 2003)

$ZnNMn_3$ has an unusual cubic-to-cubic structural phase transition near 160 K, which coincides with the onset of the antiferromagnetic (AFM) ordering. The phase transformation involves the formation of microcracks induced by the magnetic moment-dependent lattice expansion, which is also accompanied by an upturn in the resistivity curve $\rho(T)$ near the Néel temperature. With an increasing number of warming and cooling cycles, the $\rho(T)$ curve shifts to progressively higher resistivity values due to the formation of microcracks. The origin of this peculiar behavior is discussed in terms of a reduced mean-free path associated with electron scattering on cracks at constant carrier concentration. In addition, we show that the AFM alignment caused by the interatomic distance-dependent exchange inversion leads to lattice expansion.

DOI: 10.1103/PhysRevB.68.172402 PACS number(s): 75.30.Kz, 62.20.Mk, 72.15.−v, 75.80.+q

Over the past two decades or so, oxygen-based perovskite compounds with the general formula of RMO_3 (R=rare earth or alkaline element, M= transition metal) have been extensively studied given that they display a wide range of novel phenomena such as ferroelectrics,[1] superconductivity,[2] and colossal magnetoresistance.[3] In contrast, relatively little is understood about the anti-perovskite materials of AXM_3 (A=main group element, X=carbon or nitrogen) which are isostructural with the perovskite oxides.[4] Recently, however, this group and others have reported superconductivity,[5] giant magnetoresistance,[6,7] and a nearly zero temperature coefficient of resistance[8] in the metallic antiperovskites. Furthermore, we have revealed that a strong correlation among spin, charge, and lattice exists in $GaCMn_3$, implicating that various unique properties can also be found in the antiperovskite system.[7]

The simultaneous occurrence of structural change and magnetic ordering is one of the most intriguing characteristics of magnetic materials. Magnetically induced changes in the volume of these materials usually occur near the magnetic ordering temperature. This magnetostriction shows a strong dependence of the exchange interaction on the separation between the magnetic atoms. Namely, the magnetization increases or decreases with the atomic distance, which typically occurs without disrupting the structural integrity of the material. In general, the structural phase transition is reversible and closely associated with symmetry change. However, very recently, Choe *et al.* found that a crystallographic transition of $Gd_5(Si_2Ge_2)$ occurs simultaneously near the Curie temperature. A striking feature of this process is that it involves the breaking and forming of covalent bonds between Si and Ge atoms.[9]

Here we report another magnetically correlated phenomenon in the antiperovskite $ZnNMn_3$, in which the first order antiferromagnetic (AFM) ordering induces an irreversible bond-breaking transition without symmetry change. Remarkably, this results in microcracks, which are mainly due to the magnetic moment-dependent lattice expansion caused by the AFM alignment of Mn spins. At every warming and cooling cycle, the resistivity curve of $ZnNMn_3$ shifts to progressively higher value and shows an upturn near the Néel temperature T_N, which is concomitant with a cubic-to-cubic phase transition. The main purpose of this paper is to show that the large discontinuous lattice expansion is driven by the AFM ordering. In addition, we will discuss the microscopic origin of the interplay among lattice, spin, and charge in terms of charge transfer between the spin-polarized bands.

A stoichiometric mixture of Mn_2N and Zn was pressed into a pellet, which was then wrapped with tantalum foil and sealed in a quartz tube under vacuum. The sample was initially annealed at 500 °C for 40 h. After grinding the annealed sample and pressing into a pellet again, final sintering was carried out at 700 °C for 40 h, which yields a polycrystalline sample of $ZnNMn_3$. Neutron powder diffraction data

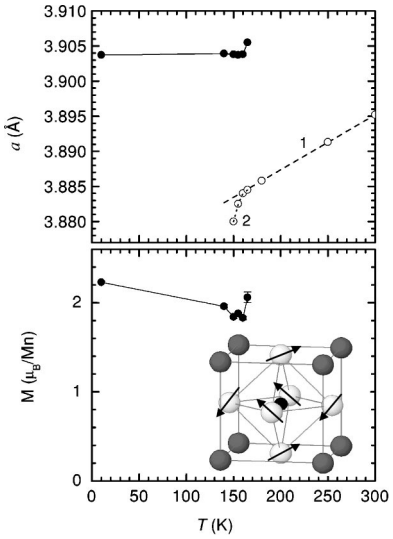

FIG. 1. The top panel shows the temperature-dependent lattice parameters of $ZnNMn_3$ obtained from neutron diffraction data. The dashed line is a linear fitting curve (1). The ordered magnetic moment and the AFM spin structure of $ZnNMn_3$ below 165 K (inset) are given in the bottom panel. Open, shaded, and filled circles represent Mn, Zn, and N atoms, respectively. Arrows indicate the directions of Mn spins.

TABLE I. Structural parameters for $ZnNMn_3$ at some temperatures. Space group is $Pm3m$ (No. 221). The Mn atoms reside at (0.5, 0.5, 0), the Zn atoms at (0, 0, 0), and the N atoms at (0.5, 0.5, 0.5). Since all the atoms are at special positions, their positions were not refined.

	300 K	180 K	165 K	165 K	160 K	160 K
a (Å)	3.8951(3)	3.88594(8)	3.8848(1)	3.9052(2)	3.8844(2)	3.9040(1)
B_{overall} (Å^2)	0.33(4)	0.08(3)	0.08(3)	0.02(16)	0.28(12)	0.08(4)
$M(\mu_B)$				2.11(8)		1.83(2)
Fract. (%)	100	100	88.4	11.6	17.1	82.9
R_p (%)	5.70	5.90	5.72	5.72	5.96	5.96
R_{wp} (%)	7.50	8.06	7.65	7.65	7.98	7.98
χ^2	1.82	2.13	1.91	1.91	2.07	2.07
	155 K	155 K	150 K	150 K	140 K	10 K
a (Å)	3.8824	3.9040(1)	3.8810(6)	3.9041(1)	3.9041(1)	3.90371(8)
B_{overall} (Å^2)	0.24(29)	0.14(3)	0.10(47)	0.28(3)	0.09(3)	0.06(2)
$M(\mu_B)$		1.87(2)		1.86(2)	1.95(2)	2.24(1)
Fract. (%)	4.9	95.1	2.5	97.5	100	100
R_p (%)	5.87	5.87	6.04	6.04	6.96	6.03
R_{wp} (%)	7.84	7.84	8.09	8.09	9.35	8.11
χ^2	2.01	2.01	2.14	2.14	2.90	2.20

were also collected at selected temperatures on a high-resolution powder diffractometer at KAERI, in which a neutron source with $\lambda = 1.8346$ Å supplied by a Ge (331) single crystal monochromator was used. The structural parameters were obtained by Rietveld refinement using the FULLPROF program.[7] Both magnetization and transport measurements were performed on a SQUID magnetometer (Quantum Design) in the temperature range from 5 to 300 K. Dark field images of cracks were recorded by means of energy-filtering (EF) transmission electron microscopy (TEM).

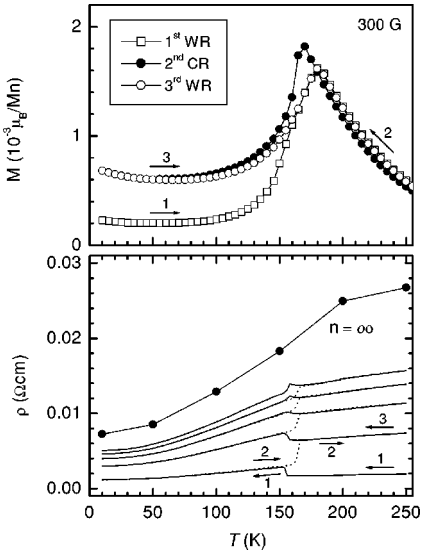

FIG. 2. Top panel shows temperature-dependent magnetization curves of $ZnNMn_3$ measured at 300 G. The open square, filled circle, and open circle represent the first warming, second cooling, and third warming runs, respectively. The bottom panel shows the temperature-dependent resistivity curves as a function of thermal cycle n. The solid and dotted lines denote the resistivity curves measured under the cooling and warming cycles, respectively. The arrow and the number indicate the direction of thermal cycle and the sequential order. Solid circles represent the calculated resistivity values as $n \rightarrow \infty$ (see text).

$ZnNMn_3$ crystallizes in the cubic perovskite structure with space group of $Pm3m$. The top panel of Fig. 1 displays lattice parameters obtained from neutron diffraction data at selected temperatures using this simple cubic model. As given in Table I, this model yields reasonable values of reliability factors. A remarkable feature is that a structural transition occurs in this system without breaking the cubic symmetry. With decreasing temperature, the lattice parameter decreases almost linearly down to 165 K (dashed line 1). Below this temperature, however, the lattice constant clearly deviates from the linearity (dotted line 2), while at the same time a new cubic phase with larger cell size (filled circle) is developed. Near 160 K the lattice parameter abruptly expands by 0.51% from 3.884 to 3.904 Å . Interestingly, the new cubic phase does not show any substantial contraction with decreasing temperature. The average ordered moment per Mn and the AFM spin structure of $ZnNMn_3$ are plotted in the bottom panel of Fig. 1. The average Mn moment is estimated to be about $2.2\mu_B$. As shown in the inset, the Mn spins located in the (111) plane form a triangular geometry with an angle of 120°, canceling out the Mn moments.[10]

The top panel of Fig. 2 shows the temperature-dependent magnetization $M(T)$ curves for $ZnNMn_3$ obtained at 300 G, in which the sample was measured for both cooling and warming cycles. A clear AFM transition is seen in both sets of data, although the Néel temperature obtained in the warming cycle shifts to a lower temperature (by about 10 K) in the cooling cycle. The thermal hysteresis in the $M(T)$ curves, particularly near T_N, implies a first order magnetic transition. As can be seen from the $M(T)$ curves, the AFM ordering occurs near the cubic-to-cubic phase boundary. More-

over, the resistivity upturn, shown in the bottom panel of Fig. 2, is also observed near T_N, indicating that a strong coupling between spin, charge, and lattice exists in the intermetallic antiperovskite system.

A remarkable feature in the transport data for this material is that the resistivity curve varies with number of thermal cycles *n*. With decreasing temperature, the initial $\rho(T)$ curve (solid line: 1) decreases almost linearly down to about 155 K, which is close to T_N, and displays an abrupt jump near that temperature, followed by a gradual reduction. Upon warming, the new resistivity curve (dashed line: 2) can be virtually superimposed on that of the initial curve (1) up to T_N. Near T_N, however, another steep rise in resistivity occurs after which the $\rho(T)$ curve shows a linear increase above this temperature. Upon subsequent cooling and warming, similar behaviors are found in the $\rho(T)$ curves. However, the magnitude of resistivity shifts to higher values as the number of thermal cycles increases. The *n*-dependent resistivity data are well fitted by the equation,[11] $\ln\rho = C_1 + C_2/n$, where C_1 is the *y*-axis intercept, which represents the resistivity value as $n \rightarrow \infty$. C_2 is the slope of the curve and represents the change in the resistivity at each thermal cycle. As can be clearly seen in the bottom panel of Fig. 2, the resistivity data (solid circle) calculated at selected temperatures converge to finite values even though n approaches infinity.

In contrast to the above, the Hall effect as well as specific heat measurements do not show any dependency on thermal cycling,[11] implicating that the charge carrier concentration is invariable. The resistivity of magnetic metal is typically expressed as $\rho(T) = \rho_0 + \rho_{\text{phonon}}(T) + \rho_{\text{magnon}}(T)$, where ρ_0 is related to impurity or lattice defects, $\rho_{\text{phonon}}(T)$ is the lattice contribution to resistivity, and $\rho_{\text{magnon}}(T)$ represents resistivity originating from magnetic interactions. Hence, only the ρ_0 component is responsible for an increase in resistivity at low temperature. Remarkably, the value of ρ_0 is drastically changed near T_N at every thermal cycle, implying that ρ_0 is associated with the irreversible structural transition. More specifically, microcracks or defects created by large irreversible lattice expansion are the main source of the resistivity upturn near T_N. The TEM image, illustrated in Fig. 3, obtained after several cooling and warming runs clearly reveals the presence of micro cracks in the lattice. Moreover, these cracks are also formed inside the regular crystal lattice marked as arrows in Fig. 3. These cracks, generated at every thermal cycle, can be considered as scattering centers of charge carriers. As a result, the ρ_0 value is enhanced with increasing number of thermal cycles.

Now we turn our attention to the origin of the crack formation, which is certainly ascribed to the lattice expansion associated with the AFM ordering. To clarify this matter, it is useful to compare temperature-dependent magnetic and lattice data of $ZnNMn_3$ with those of $GaCMn_3$. In $GaCMn_3$, both the AFM transition and the lattice expansion, given in Fig. 4, are also concurrently observed near 160 K as found in $ZnNMn_3$.[7] However, they have distinctive differences in magnitudes of magnetic moment as well as lattice change. The ordered Mn moment in $ZnNMn_3$ is estimated to be $2.2\mu_B$, which is about 2.7 times larger than that of $GaCMn_3$.

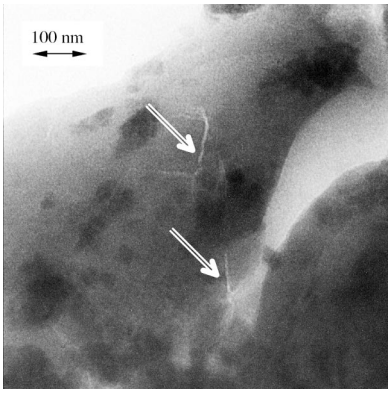

FIG. 3. Transmission electron microscopy image of cracks, indicated by arrows, obtained after several thermal cooling and warming cycles.

The large moment change near T_N in $ZnNMn_3$ might lead to irreversible lattice expansion. This subtle difference in magnetic moment leads to drastic changes in lattice parameters, which provides an important clue to understand whether structural change triggers magnetic phase transition or vice versa, which is a long-standing question in magnetoelastic materials.

It is important to note that the AFM transition of both the antiperovskites occurs at almost the same lattice constant, which is about 3.883 Å . This suggests that the magnetic transition itself is insensitive to the magnitude of the magnetic moment and Mn spin structure. Instead, the lattice change, namely, the Mn-Mn distance, triggers the AFM alignment of the Mn magnetic moment. This conjecture is supported by the fact that in $GaCMn_3$ the ordered Mn moment is virtually identical before and after the AFM transition despite the drastic change in lattice constant.

It is also known that the sign of the interlayer exchange integral strongly depends on the interatomic distance.[12] According to the exchange-inversion model, the sign of the exchange integral between the (111) planes of $GaCMn_3$, in that spins are ordered ferromagnetically within the layer, would be negative at this lattice constant, which coincides with the AFM alignment of Mn spins. It is thus conceivable that the AFM alignment leads to lattice expansion. This novel phenomenon is fundamentally different from that found in other magnetic material systems, where discontinuous structural transition is accompanied by variation in magnetic moment.[13]

Based on the data given in Fig. 4, we have argued that the lattice expansion near T_N is purely magnetic in origin. This conjecture is indirectly supported by a strong correlation between lattice parameter and ordered moment, which is presented in Fig. 5. Interestingly, the lattice parameters of $GaCMn_3$ taken from the FM region decrease with increasing magnetic moment. More importantly, the lattice parameter is proportional to the square of the spontaneous magnetization as depicted in the inset. Accordingly, the relationship between lattice and magnetization $a \propto M^2$ can be explained on the basis of an itinerant electron model.[14] Within the Stoner model, the exchange splitting of 3*d* bands yields a net magnetic moment, which also results in charge transfer between

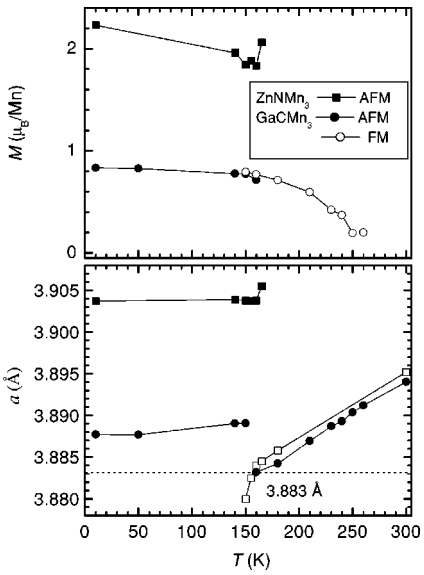

FIG. 4. Top and bottom panels show the temperature-dependent ordered moment and lattice constant of $ZnNMn_3$ (square) and $GaCMn_3$ (circle), respectively. Open and filled symbols represent ferromagnetic and antiferromagnetic states, respectively.

the majority and minority spin bands. For example, the *ab initio* band calculation on the Invar alloy Fe_3Ni reveals that an abrupt charge transfer from e_g to t_{2g} occurs at the point of magnetovolume instability.[15] In addition, thermal excitation of electrons from the antibonding majority band just below the Fermi energy level (E_F) to the nonbonding minority band just above E_F results in a reduction of the interatomic distance. This explanation on the Invar alloy can be simply extended to the antiperovskite system under discussion here. The abrupt charge transfer between the spin-polarized bands due to the AFM ordering would lead to an expanded volume near T_N. Moreover, the degree of the expansion appears to be dependent upon the magnitude of the magnetic moment. Indeed, $ZnNMn_3$ undergoes a larger volume expansion

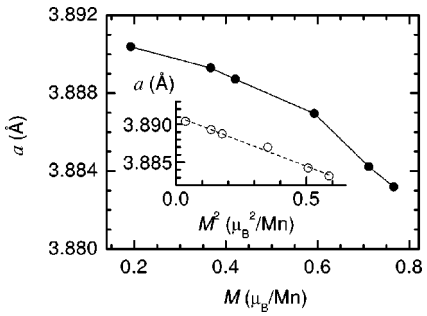

FIG. 5. Lattice constant as a function of magnetic moment M taken from the ferromagnetic range of $GaCMn_3$. The inset shows a versus M^2. The dashed line is a linear fitting curve.

(1.53%) than $GaCMn_3$ (0.45%), which agrees well with the difference in magnetization. The lattice expansion in $ZnNMn_3$ induced by the magnetic ordering is too large to maintain the structural integrity of the material, the effect of which is the appearance of crack formation.

In conclusion, in the antiperovskite $ZnNMn_3$, we have found large discontinuous expansion of lattice parameter in the vicinity of the Néel temperature. Based on our comprehensive structural, magnetic, and transport studies, we are able to postulate that the first order AFM ordering driven by the interatomic distance-dependent exchange interaction induces an irreversible structural transition that leads to the formation of cracks. Future work will address the theoretical *ab initio* calculations involving chemical bonding, as well as magnetic and elastic energy, in order to obtain a deeper insight into the relevant physics underlying crack formation associated with magnetic ordering.

We are grateful to C. S. Hong and J. H. Dho for helpful discussions. We acknowledge the Creative Research Initiative Program for the financial support provided to enable us to undertake this work.

*Email address: nhhur@kriss.re.kr

[1] C.H. Ahn *et al.*, Science **276**, 1100 (1997).
[2] J.G. Bednorz and K.A. Mueller, Z. Phys. B: Condens. Matter **64**, 189 (1986).
[3] Y. Tokura, *Colossal Magnetoresistive Oxides* (Gordon and Breach Science Publishers, Singapore, 2000).
[4] D. Fruchart and E.F. Bertaut, J. Phys. Soc. Jpn. **44**, 781 (1978); D.A. Papaconstantopoulos and W. E. Pickett, Phys. Rev. B **45**, 4008 (1992); M.Y. Chern *et al.*, J. Solid State Chem. **96**, 415 (1992).
[5] J. D. Corbett *et al.*, J. Alloys Compd. **230**, 1 (1995); T. He *et al.*, Nature (London) **411**, 54 (2001).
[6] K. Kamishima *et al.*, Phys. Rev. B **63**, 024426 (2000).
[7] W.S. Kim *et al.*, Solid State Commun. **119**, 507 (2001).
[8] E.O. Chi *et al.*, Solid State Commun. **120**, 307 (2001).
[9] W. Choe *et al.*, Phys. Rev. Lett. **84**, 4617 (2000).
[10] J.H. Shim *et al.*, Phys. Rev. B **66**, 020406 (2002).
[11] W.S. Kim, E.O. Chi, J.C. Kim, and S.J. Oh (unpublished).
[12] C. Kittel, Phys. Rev. **120**, 335 (1960).
[13] E.F. Wassermann, in *Ferromagnetic Materials*, edited by K.H.J. Buschow and E.P. Wohlfarth (North-Holland, Amsterdam, 1990), Vol. V, pp. 237–322; E.F. Wassermann, J. Magn. Magn. Mater. **100**, 346 (1991).
[14] V.L. Moruzzi, Phys. Rev. Lett. **57**, 2211 (1986).
[15] P. Entel *et al.*, Phys. Rev. B **47**, 8706 (1993).